Journal of Materials Chemistry C

Accepted Manuscript

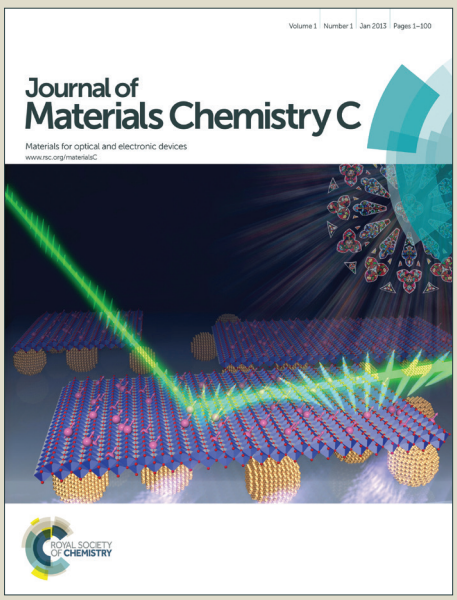

ROYAL SOCIETY OF CHEMISTRY

www.rsc.org/materialsC

Formation and selective micron-region control of PbS quantum dots inside glasses using femtosecond laser pulses

Shaohua Fan †, Guobo Wu †, Hang Zhang, Yongze Yu, Jianrong Qiu, Guoping Dong *

State Key Laboratory of Luminescent Materials and Devices and Institute of Optical Communication Materials, South China University of Technology, Guangzhou 510640, China

Abstract: Synthesis of PbS quantum dots (QDs) in solid state matrix directly and effectively is of great importance on the fabrication of PbS QDs photonic devices and their applications. Herein, the direct precipitation of PbS QDs in inorganic glass matrix through the irradiation of femtosecond (fs) laser was reported. It was demonstrated that the formation of the QDs was caused by the thermal effect of fs laser. The influence of the irradiation parameters and Ag clusters on the precipitation of QDs were investigated as well as the spatial distribution of the QDs in the irradiated area and their mechanisms. The confocal Raman spectra indicated that after irradiation the concentration of the QDs in the center is the highest. On the other hand, heat treatment processes on the irradiated sample were also carried out to adjust the size, distribution and photoluminescence of QDs in glass matrix. The electron probe micro analyzer (EPMA) provided direct evidence for the high refractive index change and the ring-shaped structure after irradiation. Based on the selective local control of PbS QDs, a waveguide demonstration experiment was conducted to illustrate the feasibility of PbS QDs waveguide directly writing with fs laser in the glass matrix.

Keywords: Optical materials; Femtosecond laser; PbS quantum dots; Waveguide; Raman spectra

† Equal contribution to this work.
* Author to whom correspondence should be addressed. E-mail address: dgp@scut.edu.cn

1. Introduction

Quantum dots (QDs) made of lead chalcogenide semiconductors can provide photoluminescence (PL) throughout the infrared band [1, 2] due to their quantum confinement [3] and they have already attracted a lot of attention for a wide range of photoluminescent [4-7] and electroluminescent [8] applications. To the moment, several host materials were proposed for PbS QD synthesis, including solid glass matrices [9-11], polymers [12, 13], organic and water solutions [14, 15], and sol-gel thin films [16, 17], etc. In particular, the glass matrix not only provide the stable matrices for QDs to prevent the agglomeration of QDs, but also can be easily formed into various shapes making the synthesis of PbS QDs in inorganic glass matrix as the perfect precursor for all-solid devices. And a number of potential applications for PbS QD-doped glasses is expanding: such as saturable absorbers for passive mode-locking [18-21], Q-switching in near-IR lasers [10, 22], and fiber amplifiers [23, 24], etc. However, one of the biggest problems that limit its application is the distribution of QDs inside the glass could not be precisely controlled because these QDs precipitate on the whole matrix usually relying on the thermal treatment. Consequently, the random distribution of QDs in glasses makes the device fabrication difficult and a well-defined distribution of functional QDs is necessary. In view of the above, several methods have been attempted to attain the controllable precipitation of QDs in glasses. Ion-Exchange was successfully used to fabricate PbS QD-doped optical waveguides in oxide glasses [25-27] and spatial control of the QDs was also achieved [28]. Even though the precipitation of the QDs can be restricted in a very narrow range (< 5 μm), the exchanged area is still a little too large which did not reach precise micron grade in three-dimensional space. In the meantime, another method ion implantation was also used to precipitate lead chalcogenide QDs in glasses [29-31]. This method can increase the concentration of QDs within a submicron layer beneath the surface of glasses, but it is also difficult to control the distribution along the thickness of the glasses. In addition, the size distribution of QDs was not pleasant and the glasses can be damaged a lot. It's worth noting that this method is difficult to realize the control of the QDs to precipitate in designated microscopic zone of the sample and the QDs can always be detected in a large plane or long channel (in millimeter scale).

Femtosecond (fs) laser which has been used to precipitate metal nanoparticles and nonlinear microcrystals in glasses [32-35] was also used to synthesize PbS QDs [36, 37]. However these reports mainly pay attention to the properties of PbS QDs from macroscopic perspective, the formation and properties of QDs haven't studied on the microscopic scale. Moreover, the micro-region analysis of the QDs is very important to the controllable synthesis and distribution of QDs in microscopic three-dimensional space. The further micro-region work on QDs can helps much for the application of QDs in micro-optoelectronic devices. On the other hand, it is already known that the formation of Ag clusters can affect the growth of the QDs [28, 38]. Thus, herein, we first report the direct micro-region precipitation of PbS QDs in glass matrix induced by fs laser. The mechanism of the formation of the QDs and the influence of the Ag clusters on the QDs was investigated systematically. Furthermore, the spatial control growth of the QDs by heat-treatment and the waveguide structure of the irradiated area were also presented.

2. Results and Discussion

2.1. Precipitation of PbS QDs under Annealing Process

Generally the annealing process is used to promote the diffusion and aggregation of Pb and S atoms, and finally leads to the formation of PbS QDs in the glasses fabricated with the conventional melting method. Figure 1 (a) and (b) show the typical absorption spectra for PbS QDs in the glasses which contain no $AgNO_3$ (NAG) and the glasses contain 20 ppm (in mol %) $AgNO_3$ (AG), respectively. Both of the two kinds of glasses were heat treated at 580 ^oC for the same durations from 3 to 20 hours. Obviously, the characteristic absorption peaks reveal that PbS QDs precipitated from both of the two glass matrixes after heat treatment [20]. The position λ_{1s} of the 1s-1s electron-hole absorption peak of these QDs in both the two glasses shifts toward longer wavelength. And the radii R of the QDs are calculated using a hyperbolic band model on the basis of the absorption peak location λ_{1s} [39]:

$$(\hbar\omega_{1s})^2 = \left(\frac{hc}{\lambda_{1s}}\right)^2 = {E_g}^2 + \left(\frac{2\hbar^2 E_g}{m^*}\right)\left(\frac{\pi}{R}\right)^2 \qquad (1)$$

where we used the room temperature T=300 K, d band gap energy of E_g=0.41 eV and effective mass of $m^*=0.12m_0$ for PbS. Table S1 in the supporting information shows the calculated results. The radii of the QDs in each kind of glasses increase with the red shift of the absorption peak which is attributed to quantum confinement effect [3]. The precipitation of PbS QDs in the two glass systems provides the fundamental premise to induce PbS QDs to separate out from the matrix with fs laser in the subsequent experiments. Besides, there are three principal disparities between the absorption spectra for AG and NAG. Firstly, the absorptance for AG was much larger than those for NAG under the same annealing conditions and it indicates the larger number density of PbS QDs formed in AG than in NAG. Represented by the absorption spectra of AG and NAG both heat treated at 580 ^oC for 20 hours, the gap between the absorptance of AG and NAG is about 0.55 cm^{-1}. The increase of the gap with the annealing duration is also shown clearly in Table S1 and the difference becomes more evident with the increase of the temperature. Secondly, the locations of the absorption peaks for NG and NAG in the early stage of heat treatment are basically the same, but the absorption peak of AG becomes shorter compared to NAG when the annealing duration reaches 10 hours and 20 hours. The PL spectra for AG and NAG after heat treatment for durations longer than 10 hours are shown in Fig. S1. For the PL peaks of AG, blue shifts were observed compared with that of NAG and it is consistent with the absorption results. All of the results demonstrate that the size of QDs in AG is smaller than that in NAG when they are annealed for sufficient durations just as the calculated radii in Table S1 indicate. Another difference is that the threshold temperature for AG when the typical absorption peak arises is lower than NAG. When they are both heat treated for 5 hours, the 1s-1s absorption peak arises at ~560 ^oC (Fig. S2 (a)) in the absorption spectra of AG, while for NAG the threshold temperature is ~580 ^oC (Fig. S2 (b)), which

is about 20 ^{o}C higher implying that the formation of PbS QDs in AG is also easier than that in NAG.

According to previous work, Ag clusters can form in the glass matrix during the annealing process which is responsible for the differences [38]. In the glass matrix, as the Ag clusters provide nucleation sites for QDs, the QDs were easier to precipitate in AG and the number density of QDs of AG increases subsequently. Furthermore, because the crystal growth in the initial stages from glass/melt is expected to be a diffusion-controlled process [40], the change of the environment of every individual QD can exert great influences on the growth of the QDs. In AG, the nucleation process completed when heat treated at 580 ^{o}C for 3 hours forming rather more QDs nucleation sites and then the growth process of QDs will dominate. At the growth stage, the final size of the QDs is determined by the concentration of Pb and S atoms around nucleus. So the smaller size of QDs observed in Fig. 1 (d) and inferred from the absorption spectra is deduced to the relatively lower concentration of Pb and S atoms around the nucleus of QDs in AG. Figure 1 (c) and (d) show the TEM micrograph of quasi-spherical PbS QDs dispersed in the two kinds of glassy matrix heat-treated at 580 ^{o}C for 20 hours. Histograms of the size distribution of the QDs are shown in Fig. 1 (e) and (f), with an average diameter of about 7.1 nm and 5.4 nm, respectively. They are a little bigger than the diameters in Table S1. This is probably caused by the QDs' low degree of crystallinity. As one can see, the QDs density in AG is higher than that in NAG, but the average size is much smaller. The TEM results give a further demonstration on the deductions from the absorption and PL spectra.

The fs laser irradiated area can be as small as only a dozen microns [41], and the confocal micro-Raman spectra can detect a region as small as ~1 μm which helps much for the characterization in the micro-region. Therefore, the Raman spectra of the as-prepared and heat-treated glasses were shown in Fig. 2. And all of the Raman spectra in this work were for

785nm excitation. For the two as-prepared glasses, there both exist three main peaks locating at 1375 cm^{-1}, 1670 cm^{-1} and 1840 cm^{-1} in the Raman spectra. The broad band near 1375 cm^{-1} is attributed to the $BØ_2O^-$ triangles linked to $BØ_4^-$ units (Ø: oxygen atom bridging two boron atoms and O^-: non-bridging oxygen atom) [42-45]. The broad bands above 1600 cm^{-1} in the spectra of the glasses probably due to moisture (the bending mode of H_2O is at approximately 1600 cm^{-1}) and they may also arise from B-O stretching modes involving mostly BO_3 triangles with one non-bridging oxygen as 1375 cm^{-1} [46]. During the heat treatment process, the intensities of 1840 cm^{-1} and 1670 cm^{-1} to that of 1375 cm^{-1} both increases. This assigned to the enhancement of the fluorescence background caused by the PbS QDs formed during the annealing process. According to the Stokes shift, when the fluorescence of PbS QDs is between 850~975 nm (close to the detection limit of charge-coupled device (CCD) used in Raman spectrometer), the Raman shift is 1000 cm^{-1} to 2500 cm^{-1}. Thus the relative intensities of 1840 cm^{-1} and 1670 cm^{-1} to 1375 cm^{-1} were affected a lot by the fluorescence background. And the longer the annealing duration is, the more the PbS QDs precipitate together with the increasing relative intensities of 1840 cm^{-1} and 1670 cm^{-1} to 1375 cm^{-1}. Moreover, the annealing time for AG when the Raman spectra totally exhibit fluorescence spectra characteristic differs from that of NAG. When NAG is heat treated at 560 ^oC for 10.5 hours, a fluorescence peak centered at about 1775 cm^{-1} was observed in Raman spectra. While for AG the duration is only 4.5 hours and it is much shorter. Besides, the fluorescence peak of it centered at about 1988 cm^{-1} in the even longer wavenumber shown in Fig. 2 (b). In all, the Raman result is consistent with the conclusion that QDs were easier to precipitate in AG deduced from the absorption spectra in Fig. S2.

Compared with the absorption spectra, the confocal micro-Raman spectra were more sensitive to the formation of PbS QDs. For instance, during the annealing process, the absorption spectra in Fig.

1 (a) and (b) show no obvious changes except a tiny red shift of the absorption edge until a small absorption peak arises at last, while the shapes and positions of the Raman spectra in Fig. 2 experienced great changes. So in the next section followed by the experiment of irradiating the glasses with fs laser, the confocal micro-Raman spectra as a powerful probe are utilized as the most principal technique to study the changes of the samples.

2.2. Precipitation of PbS QDs Induced by Fs Laser

On the basis of the investigation on the QDs in the glasses with heat treatment, the glass matrixes were irradiated with fs laser pulses. Details of the experiment can refer to the Experiment section in the supporting information. The Raman spectra of the irradiated area in NAG with laser powers 1.2 W, 1.5 W and 1.8 W are shown in Fig. 3 (a), (b) and (c) respectively and the Raman spectra for the dots detected in the figures were arranged based on the distance to the center. The confocal center is labeled as 0 μm, and the other dots detected were selected every 5 μm across the radius of the irradiated area. Figure S3 shows the optical microscope images captured after laser irradiation with different pulse energy. As is easily seen, regular ring-shaped patterns with diameter ranged from 125 to 235 μm caused by the changes in refractive index are clearly around the focal point indicating the uniform changes around the center. Thus, to some extent the line scanning mode used in our Raman detecting can make an insight of the changes of the whole area. As we can see, all of the samples show similar Raman spectra. When the distance to the irradiation center exceed 20 μm (Fig. 3 (a), (b) and (c)), the Raman spectra for different samples are all identify to that of the as-prepared NAG (Fig. 2 (a)). This implies that when the distance to the irradiation center is large enough, the influence of the laser on the glass matrix can be neglected. However, with the decreasing of the distance to the irradiated center, the shape and the intensity of the Raman spectra changed dramatically. In particular, the relative intensities between the three main Raman peaks mentioned above changes. Taken the intensity of the peak at 1840 cm^{-1} to that of peak at 1375 cm^{-1} for example, it is clear that the relative intensity between the two peaks is a function of the distance to the irradiation center. The closer to the center, the larger the intensity ratio of the peak 1840 cm^{-1}

to that of 1375 cm^{-1}.And the same phenomena were observed when the area was irradiated with different laser power. The change of the Raman spectra shows a distance-related characteristic similar to the change of the Raman spectra for the samples after heat treatment which exhibit a duration-related characteristic. The comparable changes between the heat treated and the irradiated samples indicates that nanostructured PbS QDs may also precipitate in the irradiated area because the irradiation center also shows florescence as NAG do when it is heat treated at 560 ^{o}C for 10.5 hours. Thus all of the changes in the Raman spectra were deduced to the enhancement of fluorescence background of PbS QDs. Different to the growth of PbS QDs during the heat treatment process, the thermal effect of laser irradiation instead of heat treatment plays an important role in the process of PbS QDs growth. According to previous study [47], various structures can be produced by using pulsed laser operating at the non-resonant wavelength with pulse widths of the order of femtoseconds. The structure character observed in this work (Fig S3 and S4 shown in ESI) resembles the structure in previous study [47]. Thin kind of structure is due to avalanche ionization caused by the multiphoton absorption. In such process, avalanche ionization produces highly absorptive and dense plasma, facilitating the transfer of energy from the laser to the glass. The resulting melting, material displacement resulted into the structure here. Herein, we interpreted it as the thermal effect of fs laser. Thus the thermal effect around the irradiated area is so strong which will promote the bonding of Pb^{2+} and S^{2-} to form PbS QDs. Furthermore, by comparing Fig. 3 (a), (b) and (c), it is seen that the intensities of the 1840 cm^{-1} peak for the irradiated dots 10 μm from the center (shown in Fig. 3 (d)) increase with laser power. As we all know, the thermal effect of laser during the irradiation process is affected directly by laser power, the higher the laser power is, and the more obvious the thermal effect can exhibit. So the enhanced thermal effect results in promoting the precipitation of PbS QDs and the increase of the relative intensity of the 1840 cm^{-1} to 1375 cm^{-1} peak. Moreover, this result also revealed that the area with the precipitation of PbS QDs spread in higher laser power which is consistent with the increase of the diameter of the fs laser induced zone observed from the optical microscope images.

AG glasses were also irradiated by fs laser with same parameters to that of NAG and the Raman

spectra of their irradiated area are shown in Fig. 4. Corresponding optical microscope images are arranged in Fig. S4. The locations of the Raman peaks in the Raman spectra of the two as-prepared glasses are basically identical and the relative intensities of these peaks shows a same change trend with the distance to the irritation center. However, the relative intensity of the Raman peak 1840 cm^{-1} inversely decrease with the laser power presented in Fig. 4 (f) (the data were collected form Fig. 4 (a), (b) and (c)). Similarly, Fig. 4 (a), (d) and (b), (e) show that the scanning speed also has an effect on the intensities of 1840 cm^{-1} peak, the higher scanning speed causes the drop of the intensities of the 1840 cm^{-1} peak. They both suggest that PbS QDs precipitating area decreased. The decrease of the area may be caused by the enhancement of the micro-explosion which can promote Pb^{2+} and S^{2-} farther from the center. Finally the zone where QDs formed shrank. Moreover, the increase of the laser power surprisingly accompany a blue shift of the Raman peak for the irradiated center as shown in Fig. 4 (f) and this implies that the size of the PbS QDs decrease with the increase of laser power. While for NAG, no apparent shift was observed. This difference is owing to the addition of Ag in the glass. For AG, in the irradiation process, Ag clusters form in the initial stage as the nucleating centers of PbS QDs. The higher the laser power, the more the cluster forms. Thus when Pb^{2+} and S^{2-} migrated to Ag clusters forming PbS QDs, the competition between the Ag clusters becomes fiercer resulting in the decrease of the size of PbS QDs. The opposite change trend for NAG and AG is because the balance of element-migration and QDs formation process is different. The existence of the balance can be proved from the increase of the 1840 cm^{-1} relative intensity at 25 μm when irradiated with 1.8W at 5 μm/s for NAG (Fig. 3 (c)) and AG (Fig. 4 (c)). And it will be discussed in detail in the next section.

So it is clear that PbS QDs were both induced to precipitate with fs laser power in NAG and AG. The growth of the Pb QDs can be affected by the laser irradiated parameters such as the laser power

and scanning speed, but the addition of $AgNO_3$ distinguishes their influences in NAG and AG. Given the results obtained in the analysis of Ag effect on the QDs after annealing in the preceding section, the influences of the irradiated laser power is similar to the heat treat temperature. The influence of scanning speeds which correspond to different irradiated durations is similar to the heat-treat durations.

2.3. Micro-region structure and elements analysis of the irradiated region

2.3.1. Micro-region Structure Analysis

In the foregoing Raman spectra analysis of the fs laser irradiated area, only the line scanning detect was used on the presupposition that the changes is uniform when scanned from the center to the outer space in different directions. Given that, reliable and first hand spatial detect is needed to make a clear observation of the changes in the whole area. Besides, it is important to point out that all of the intensities in the Raman spectra as already shown in the foregoing section are relative intensity to that of the Raman peak at 1375 cm^{-1}, so the information about the actual distribution of the PbS QDs revealed through the absolute Raman intensity was neglected. Therefore a further detect by means of the Raman mapping, i.e., analysis of x-y plane using confocal Raman microscopy (Shown in Fig. 5) was conducted in order to make a detailed investigation in the definite spatial distribution of the formed PbS QDs and the change of the glass matrix in the irradiated area. The AG glasses irradiated with laser power 1.8 W at speed of 5 μm/s, containing the most visible and dramatic information about QDs, was chosen to perform the test and three representative Raman bands locating at 1375 cm^{-1}, 1840 cm^{-1} and 2300 cm^{-1} were characterized with Raman mapping. Figure 5 (a) shows the optical photo captured by an optical microscope. Due to the very close location of the Raman peak at 1375 cm^{-1} and 1840 cm^{-1} and the fluorescence peak shown in the Raman spectra mentioned above, the spatial variation of the intensities of 1375 cm^{-1}

and 1840 cm^{-1} cannot directly reveals the concentration profile of the formed PbS QDs in the irradiated area. The Raman band at 2300 cm^{-1} locates at the band tail of the fluorescence peak and no Raman peak ascribed to glass matrix arises. Hence the variation of its intensity perfectly represents the distribution of PbS QDs.

As one can see, the center (Area A in Fig. 6 (a)), which is labeled as the red area in Fig. 5 (b), has the strongest Raman intensity in the whole area and it confirmed the highest PbS QDs concentration in the center. In area B (Fig. 6 (a)) which diverges a little from area A and it is labeled as purple color in Fig. 5 (b), the Raman intensity keeps reducing. When the area location (referred to area C in Fig. 6) is farther than that of the area B, an increase of the Raman intensity was observed with the change of the colors from purple to green. This implies that B area has the lowest PbS QDs concentration in the whole area. The intensity distribution of Raman mapping image (Fig. 5 (c)) for 1840 cm^{-1} is identical to that for 2300 cm^{-1}. In Fig. 5 (d), the spatial intensity of 1375 cm^{-1} also varies in the same nature with the 2300 cm^{-1} and 1840 cm^{-1} peak confirming the rather weak influence of the Raman scattering signal on the fluorescence intensity. The mapping for 1840 cm^{-1} and 1375 cm^{-1} makes a supplementary confirmation of our analysis results for 2300 cm^{-1}. All of the Raman mapping results indicates that the concentration of the PbS QDs in area B is the lowest. As the bonding of Pb^{2+} and S^{2-} when forming PbS QDs is induced by the thermal effect of fs laser, the further the distance to the irradiated center, the weaker the thermal effect exhibits. And the too weak thermal effect is not beneficial for the *in situ* bonding of Pb^{2+} and S^{2-}. Thus it was thought that the QDs' concentration in area C should be the lowest. However, the element-migration process also takes place and it trends to make the QDs precipitate in the area far from the center resulting in an adverse PbS QDs concentration gradient to that of the *in situ* bonding process. Thus after irradiation the area with the lowest PbS QDs concentration is rather not area C but area B where the two

process balance. These results are consisted with the abnormal increase of the 1840 cm^{-1} relative intensity at 25 μm for NAG (Fig. 3 (c)) and AG (Fig. 4 (c)). And the increase was only observed when irradiated with 1.8 W. All of other samples irradiated at 1.2 W and 1.5 W with different speed do not behave like this. It is probably that the *in situ* bonding process of Pb^{2+} and S^{2-} is dominating for the formation of QDs when irradiated at small energy (1.2 W and 1.5 W), while for the samples irradiated with stronger energy (1.8 W), the element-migration process, also caused by thermal effect of fs laser, is significant enough to influence the final distribution of the QDs. To the best of our knowledge, the element-migration process has been reported in several glass matrix systems when irradiation with fs laser [48-50]. And the effect of the element-migration process will be discussed in detail in the next section.

2.3.2. Micro-region Element Analysis

As one of the nondestructive testing technologies, EPMA is used to analysis the change in the composition of the samples which remained intact throughout the analysis. The element analysis was conducted with the line scanning model across the diameter of the irradiated area using the EPMA-1600 (Shimadzu, Japan). The sample used for detecting is irradiated with laser power 1.8 W at speed of 5 μm/s, which is the same to that in the Raman mapping characterization. Figure 6 (b) shows the radial direction distribution of all the elements contained in the glass matrix. Given that the irradiated zone in Raman mapping have a radial symmetry, the element line scanning results here also give an insight of a two-dimensional spatial distribution of the elements. It is noteworthy that the concentration of the ions Pb^{2+} and S^{2-} used to form PbS QDs experience great changes. As Pb^{2+} contents in the glass matrix is rather low which is only 1 % nominally, it is also classified as glass modifier. Furthermore, the single-bond strength of Pb-O is about 36 kcal/g atom [51], which is low enough to diffuse away from the focal point. The identify change of S^{2-} with Pb^{2+} is attributed

to its partiality to combine with Pb^{2+} [52] [53]. As a result, the PbS formation ions (Pb^{2+}, S^{2-}) in the focal center is the least and area B have the highest concentration. So element-migration process and the *in situ* bonding process of Pb^{2+} and S^{2-} were both caused by the thermal effect during the irradiation. And the working together of them finally determined the distribution of PbS QDs in the irradiated area. Due to element-migration, the concentration of Pb^{2+} and S^{2-} is rather low in the focal center area A and it is unfavorable for the *in situ* bonding and the growth of PbS QDs. In area B, though the concentration of Pb^{2+} and S^{2-} is relatively high, the weak thermal effect, owing to the long distance from the irradiation center, depresses the formation of PbS QDs. All in all, the element-migration and the *in situ* bonding of Pb^{2+} and S^{2-} have converse influence on the spatial distribution trend of PbS QDs as we surmised in the Micro-Region Structure Analysis Section by Raman-Mapping. Finally the balance of the two processes makes the concentration of QDs in area B is the lowest. These results can only be observed when irradiated at relative high energy. The threshold energy is between 1.5 W and 1.8W.

In Fig. 6 (b), the relative concentrations of Si^{4+} and O^{2-} ions (termed group I ions) increase and those of K^{+}, Zn^{2+}, B^{3+} (termed group II ions) decrease at the focal point. However, in the area around the focal point, an opposite trend is observed. The blue (B) and yellow (C) areas correspond to a circular area with a radius of 10 μm and around the focal point with a radius of 18 μm, respectively. In the blue area B, the concentrations of Si^{4+} and O^{2-} ions increase sharply and the concentration of Group II ions, especially Zn^{2+} decreases. Besides, the concentrations of group I ions decrease and those of group II increase in the yellow area C. Thus, besides the dramatic changes in the focal center, there is also obvious migration of elements between area B and C. The different ion distribution profiles for Groups I and II may be attributed to the behavior of each ion in the glass [48]. Detail discussion about the migration of Si, O, K, Zn and B are shown in the

supporting information.

As we all know, the refractive index of the glass directly relates to the content of each element, thus the ring-shaped structure of the glass around the focal point indicates a high refractive index change. Then it is inferred that a waveguide structure (high refractive index in A and relative low refractive index in B and C) was formed in the irradiated area. The end-face coupling method was conducted to confirm it. A sketch of the end-face coupling experiment setup is shown in Fig. 7 (a). Figure 7 (b) shows the microscope image in end view and the near-field intensity distribution of waveguides can also be distinguished. Clearly the intensity in the center is much stronger than the surrounding area illustrating that a guided mode occurs in the center. However, the glass used to fabricate the waveguide was not homogeneous enough. Finally, the beam quality is too poor to identify whether it is single mode. More work on the improvement of the waveguide quality is needed.

2.4. Controlled precipitation of PbS QDs in the irradiated region

Obviously, for both of the two kinds of glasses distinguished on whether they contain $AgNO_3$, PbS QDs can precipitate under fs laser pulses. And to the best of our knowledge, the tunable of the fluorescence band is one of the key factors which determine the application of PbS QDs. It is also of great significance to regulate the fluorescence characteristic of the PbS QDs precipitated in the irradiated micron-region. However, the fluorescence shift which is only ~200 cm^{-1} for the biggest shift shown in Fig. 3 and Fig. 4. Thus a further study was carried out on the controlled precipitation of PbS QDs in the irradiated region through the most commonly used heat treatment method. Detailed discussion about the mechanism of the changes will be given as follows.

On the basis of the investigation about Ag effect on the PbS QDs (see Section 2.1), it is demonstrated that the AG glasses is more sensitive to the annealing process and it is easier to

control the QDs in the glasses. The Raman spectra of AG can exhibit entirely fluorescence background of PbS QDs when heat-treated at 560 ^{o}C for 4.5 hours (Fig. 2 (b)). This time is too short to make detail studies. Thus the annealing temperature was reduced to 540 ^{o}C. First of all, the Raman spectra of the non-irradiated AG annealed at 540 ^{o}C with different duration were presented in Fig.8. As an illustration, the Raman spectra in Fig. 8 did not show obvious florescence character (which is indicated by the increase of the intensity of the Raman peak at 1840 cm^{-1}) until the sample was annealed for 10 hours. After annealed for 20 hours, the Raman spectra exhibit totally florescence background. Thus the operating time can be as long as at least 10 hours which assures the characterization precision. And AG irradiated with laser power 1.8 W and scanning speed 5 μm/s were heat-treated at 540 ^{o}C for 5 and 7.5 hours and corresponding Raman spectra were shown in Fig. 9, respectively. Obviously, after heat-treated the Raman spectra of the samples show stupendous changes and much more spatial dependence while the un-irradiated area remains unchanged. This dramatic contrast is caused by the thermal effect of fs laser as we discussed before. Some QDs nucleus formed and the distribution of the ions changed in the irradiated area. Finally, the irradiated area is much more sensitive to the annealing than the un-irradiated area. This makes the restricted control of the QDs only in the irradiated area possible. When heat-treated for 5 hours, the spectrum for the focal center in Fig. 9 (a) demonstrates little changes of the irradiated center of the sample. The wavelength of the peak remains constant indicating that no further growth happened to the primal PbS QDs induced by the fs laser, and the possible reasons will be discussed subsequently. With the increase of the distance to the center, the Raman spectra change significantly on the whole. Compared with the spectra for the corresponding spectra in Fig. 4 (c) without annealing, the spectra in Fig. 9 (a) for the dots 5 μm, 10 μm and 15 μm far from the center show stronger fluorescence background of PbS QDs. The Raman spectra at 20 μm, 25 μm exhibit so

strong fluorescence of PbS QDs that the spectra are absolutely fluorescence spectra character which can be deduced to the high concentration of Pb and S elements in this area demonstrated in the Micro-Region Element Analysis Section. There also exists a red shift from the spectrum of 20 μm to that of 25 μm.

The *in situ* growth of PbS QDs in the irradiated area can be affected by the concentration of the primitively formed nuclei and the concentration of the surrounding ions. And the concentration of the QDs' formation ions plays a principal role. For the focal center, the concentration of PbS nuclei is the highest, but the Pb^{2+} and S^{2-} concentration is the lowest. Consequently, in spite of its initial high PbS nuclei concentration, the nuclei is difficult to grow with low concentration of PbS formation ions during the heat-treated process and this is consist with the constant Raman spectrum at 0μm and the Micro-Region Element Analysis results in Fig. 6. For the area from 5 μm to 20 μm far from the irritation center, due to the low concentration of PbS nuclei and concentration of PbS formation ions, the nuclei is even hard to get a conspicuous grow which only exhibits an enhancement of the fluorescence background of PbS QDs. In the area 20 μm to 25 μm far from the irritation center (Area B in Fig. 6), the highest concentration of PbS forming ions plays a dominant effect on the formation and growth of the QDs, thus the Raman spectra for this area show absolutely fluorescence character. The peak location is in the even longer wavelength with about 400-700 cm^{-1} red shift. As for the Raman spectrum for 30 μm, it performed the fluorescence background again, which is because the formed PbS nuclei decrease with the increase of the distance to the center. When the distance to the irradiated center is longer than 35 μm, the concentration of the PbS nuclei and the PbS formation ions are both too low for the nuclei to generate in the matrix under annealing, so the Raman spectra behave the same as the area without laser irradiation as the Raman spectrum for annealed AG without irradiation at 540 ^{o}C for 5 hours in Fig. 8.

After annealed at 540 ^{o}C for 5 hours, it is obvious that the irradiated area have undergone tremendous changes while the un-irradiated area still maintain unchanged, thus we increase the annealing duration to 7.5 hours to make further investigation and the results were presented in Fig. 9 (b). As shown, the change trend is consistent with the samples annealed for 5 hours. The Raman peak location in the irradiated center still did not change, and the area where the Raman peak shows absolutely fluorescence spectra extended in two directions which started from 10 μm and ended at 35 μm far to the irradiated center and this indicates that more PbS QDs formed under annealing for 7.5 hours. At the area from 10 μm to 15 μm with medium concentration of primary induced PbS nuclei but few formation ions, the enhanced thermal effect for 7.5 hours durations will promote to get more and larger PbS QDs compared with that annealed for 5 hours. Similarly, the area from 30 μm to 35 μm with many formation ions but low concentration of primary induced PbS nuclei can also separate out more PbS QDs than the corresponding area annealed for 5 hours. For the area 40 μm to 50 μm far to center, the Raman spectra finally exhibit the same as the un-irradiated area heat-treated for 10 hours at the same temperature shown in Fig. 8. But as is easily seen, the relative intensity of the Raman peak 1840 cm^{-1} for this area increased indicating the stronger influence of the fluorescence background. That is to say, with longer annealing duration than 7.5 hours the micro-region local control of the growth of the PbS particles is no longer eligible. All of the results reveals that though in the irradiated center the most PbS nuclei is induced to form, a further growth is hard to obtain for them even in the strong annealing process due to the negative effect of the ion mobility process occur simultaneously. It also indicates the ion mobility plays a strong effect on the formation and growth of PbS QDs continuously throughout the irradiated area, especially in the area after a few microns from the irradiated center. That is in this area which exactly refers to area B in Fig. 6 (a), the PbS QDs are more easily to separate out from the glass matrix than the irradiated

center (Area A in Fig. 6 (a)) and the area farther than area B from the irradiated center which refers to area C in Fig. 6 (a). Furthermore, for area B the red shifts of the fluorescence peak were also observed when heat-treated at 540 ^{o}C for different durations which implies that the precisely local micro-region control of the growth of PbS particles in area B is more feasible. So the local micro-region precise control of the formation and distribution of PbS QDs in the irradiated region with the non-irradiated region remaining unchanged was successfully realized. This will make a further promotion on its practical application such as the fabrication of new photonic micro-devices with fs lasers.

For example, once high quality waveguide is fabricated with PbS QDs precipitating in it, the "postoperative" thermal treatment of the waveguide can easily regulate the output optical band maintaining its high quality. Most importantly, the devices fabricated with fs lasers are in micro-scale and then the miniature single device can be realized. Furthermore, array components can also be fabricated based on the single device.

3. Conclusion

In conclusion, PbS QDs were directly induced to precipitate in borosilicate glasses using fs laser pulses and selective local micro-region precise control of PbS QDs in glasses was also realized with extra heat treatment. The confocal fluorescence Raman spectra demonstrate that after irradiation the concentration of the PbS nuclei in the center is the highest due to the combination of Pb^{2+} and S^{2-} ions caused by the strongest thermal effect of the fs laser. The micro-region Element-analysis of the irradiated area reveals the element redistribution process results in a ring-shaped structure, which indicates a high refractive index change. Base on this, a waveguide demonstration experiment was conducted successfully confirming the feasibility of direct writing PbS QDs waveguide with fs laser in the glass matrix. At the same time, the QDs' precipitation distribution and size control can be restricted only in the irradiated area through annealing the irradiated samples. The location of the

fluorescence peak shows a dependence on the annealing duration indicating that the precise micro-region control of the fluorescence characteristics of PbS QDs waveguide can also be achieved. These are of great significance in the fabrication of PbS QDs optoelectronic micro -devices and the fabrication can be even controllable considering different applications.

Supporting Information for this article is available.

Acknowledgements. This work was supported by the Guangdong Natural Science Foundation for Distinguished Young Scholars (2014A030306045), the National Natural Science Foundation of China (51102096, 61475047), the project of Guangzhou Pearl River Science and Technology New Star (2014J2200083).

References

[1] L. Bakueva, I. Gorelikov, S. Musikhin, X. S. Zhao, E. H. Sargent, and E. Kumacheva, Adv. Mater. **16**, 926-929 (2004).

[2] J. J. Peterson, and T. D. Krauss, Nano Lett. **6**, 510-514 (2006).

[3] F. W. Wise, Acc. Chem. Res. **33**, 773-780 (2000).

[4] K. R. Choudhury, Y. Sahoo, S. J. Jang, and P. N. Prasad, Adv. Funct. Mater. **15**, 751-756 (2005).

[5] M. A. Zhukovskiy, A. L. Stroyuk, V. V. Slivalagin, N. R. Smirnova, O. S. Lytvyn, and A. M. Eremenko, Journal of Photochemistry and Photobiology a-Chemistry **203**, 137-144 (2009).

[6] A. A. R. Watt, P. Meredith, J. D. Riches, S. Atkinson, and H. Rubinsztein-Dunlop, Curr. Appl Phys. **4**, 320-322 (2004).

[7] Z. Wang, S. Qu, X. Zeng, C. Zhang, M. Shi, F. Tan, Z. Wang, J. Liu, Y. Hou, F. Teng, and Z. Feng, Polymer **49**, 4647-4651 (2008).

[8] L. Bakueva, S. Musikhin, M. A. Hines, T. W. F. Chang, M. Tzolov, G. D. Scholes, and E. H. Sargent, Appl. Phys. Lett. **82**, 2895-2897 (2003).

[9] P. Yang, C. F. Song, M. K. Lu, X. Yin, G. J. Zhou, D. Xu, and D. R. Yuan, Chem. Phys. Lett.

345, 429-434 (2001).

[10] A. M. Malyarevich, I. A. Denisov, V. G. Savitsky, K. V. Yumashev, and A. A. Lipovskii, Appl. Opt. **39**, 4345-4347 (2000).

[11] K. Wundke, S. Potting, J. Auxier, A. Schulzgen, N. Peyghambarian, and N. F. Borrelli, Appl. Phys. Lett. **76**, 10-12 (2000).

[12] A. Stavrinadis, R. Beal, J. M. Smith, H. E. Assender, and A. A. R. Watt, Adv. Mater. **20**, 3105-3109 (2008).

[13] A. Watt, T. Eichmann, H. Rubinsztein-Dunlop, and P. Meredith, Appl. Phys. Lett. **87**, 253109 (2005).

[14] J. Tang, K. W. Kemp, S. Hoogland, K. S. Jeong, H. Liu, L. Levina, M. Furukawa, X. Wang, R. Debnath, D. Cha, K. W. Chou, A. Fischer, A. Amassian, J. B. Asbury, and E. H. Sargent, Nat. Mater. **10**, 765-771 (2011).

[15] W. Lin, K. Fritz, G. Guerin, G. R. Bardajee, S. Hinds, V. Sukhovatkin, E. H. Sargent, G. D. Scholes, and M. A. Winnik, Langmuir **24**, 8215-8219 (2008).

[16] A. Martucci, J. Fick, S. E. LeBlanc, M. LoCascio, and A. Hache, J. Non-Cryst. Solids **345**, 639-642 (2004).

[17] S. H. Wang, and S. H. Yang, Langmuir **16**, 389-397 (2000).

[18] V. G. Savitski, N. N. Posnov, P. V. Prokoshin, A. M. Malyarevich, K. V. Yumashev, M. I. Demchuk, and A. A. Lipovskii, Applied Physics B-Lasers and Optics **75**, 841-846 (2002).

[19] A. A. Lagatsky, A. M. Malyarevich, V. G. Savitski, M. S. Gaponenko, K. V. Yumashev, A. A. Zhilin, C. T. A. Brown, and W. Sibbett, IEEE Photonics Technol. Lett. **18**, 259-261 (2006).

[20] P. T. Guerreiro, S. Ten, N. F. Borrelli, J. Butty, G. E. Jabbour, and N. Peyghambarian, Appl. Phys. Lett. **71**, 1595-1597 (1997).

[21] A. A. Lagatsky, C. G. Leburn, C. T. A. Brown, W. Sibbett, A. M. Malyarevich, V. G. Savitski, K. V. Yumashev, E. L. Raaben, and A. A. Zhilin, Optics Communications **241**, 449-454 (2004).

[22] J. F. Philipps, T. Topfer, H. Ebendorff-Heidepriem, D. Ehrt, R. Sauerbrey, and N. F. Borrelli, Applied Physics B-Lasers and Optics **74**, 285-285 (2002).

[23] X. L. Sun, L. B. Xie, and W. Zhou, Optoelectronic Devices and Integration Iv **8555**, (2012).

[24] C. Liu, and J. Heo, International Journal of Applied Glass Science **4**, 163-173 (2013).

[25] J. M. Auxier, M. M. Morrell, B. R. West, S. Honkanen, A. Schülzgen, N. Peyghambarian, S. Sen, and N. F. Borrelli, Appl. Phys. Lett. **85**, 6098 (2004).

[26] J. M. Auxier, S. Honkanen, M. M. Morrell, M. A. Leigh, S. Sen, N. F. Borrelli, and A. Schulzgen, J. Appl. Phys. **99**, 126101 (2006).

[27] J. M. Auxier, S. Honkanen, A. Schulzgen, M. M. Morrell, M. A. Leigh, S. Sen, N. E. Borrelli, and N. Peyghambarian, J Opt Soc Am B **23**, 1037-1045 (2006).

[28] K. Xu, and J. Heo, J. Non-Cryst. Solids **358**, 921-924 (2012).

[29] R. Espiau de Lamaëstre, and H. Bernas, J. Appl. Phys. **98**, 104310 (2005).

[30] R. E. de Lamaestre, and H. Bernas, Nuclear Instruments & Methods in Physics Research Section B-Beam Interactions with Materials and Atoms **257**, 1-5 (2007).

[31] H. Bernas, and R. E. de Lamaestre, Ion-Beam-Based Nanofabrication **1020**, 101-108 (2007).

[32] H. Zeng, J. Qiu, X. Jiang, C. Zhu, and F. Gan, J. Phys.: Condens. Matter **16**, 2901-2906 (2004).

[33] J. Shin, K. Jang, K.-S. Lim, I.-B. Sohn, Y.-C. Noh, and J. Lee, Appl. Phys. A **93**, 923-927 (2008).

[34] W. Jie, X. Chen, D. Li, L. Xie, Y. Y. Hui, S. P. Lau, X. Cui, and J. Hao, Angew. Chem. **127**, 1201-1205 (2015).

[35] G. Bai, M.K. Tsang, and J. Hao, Adv. Optical Mater. **3**, 431-462 (2014).

[36] C. Liu, Y. K. Kwon, J. Heo, B. H. Kim, and I.-b. Sohn, J. Am. Ceram. Soc. 1221-1224 (2009).

[37] G. Badenes, G. C. Righini, I. Banyasz, S. Berneschi, M. Brenci, A. Chiasera, M. Cremona, D. Ehrt, M. Ferrari, R. M. Montereali, G. Nunzi Conti, S. Pelli, S. Sebastiani, C. Tosello, D. Abbott, and A. Serpenguzel, Proc. SPIE 5840, Photonic Materials, Devices, and Applications **5840**, 649-657 (2005).

[38] K. Xu, C. Liu, S. Dai, X. Shen, X. Wang, and J. Heo, J. Non-Cryst. Solids **357**, 2428-2430 (2011).

[39] I. Kang, and F. W. Wise, J Opt Soc Am B **14**, 1632-1646 (1997).

[40] S. Joshi, S. Sen, and P. C. Ocampo, J. Phys. Chem. C **111**, 4105-4110 (2007).

[41] J. Song, X. S. Wang, X. Hu, Y. Dai, J. R. Qiu, Y. Cheng, and Z. Z. Xu, Appl. Phys. Lett. **92**, 092904 (2008).

[42] E. Malchukova, B. Boizot, D. Ghaleb, and G. Petite, J. Non-Cryst. Solids **352**, 297-303 (2006).

[43] R. C. Lucacel, C. Marcus, V. Timar, and I. Ardelean, Solid State Sci. **9**, 850-854 (2007).

[44] T. Furukawa, and W. B. White, Journal of Materials Science **16**, 2689-2700 (1981).

[45] D. A. McKeown, I. S. Muller, A. C. Buechele, I. L. Pegg, and C. A. Kendziora, J. Non-Cryst. Solids **262**, 126-134 (2000).

[46] C. F. Windisch, E. M. Pierce, S. D. Burton, and C. C. Bovaird, J. Non-Cryst. Solids **357**, 2170-2177 (2011).

[47] J. Qiu, Chem. Rec. **4**, 50-58 (2004).

[48] S. Kanehira, K. Miura, and K. Hirao, Appl. Phys. Lett. **93**, 023112 (2008).

[49] Y. Liu, B. Zhu, L. Wang, J. Qiu, Y. Dai, and H. Ma, Appl. Phys. Lett. **92**, 121113 (2008).

[50] F. F. Luo, B. Qian, G. Lin, J. Xu, Y. Liao, J. Song, H. Y. Sun, B. Zhu, J. R. Qiu, Q. Z. Zhao, and Z. Z. Xu, Opt. Express **18**, 6262-6269 (2010).

[51] W. D. Kingery, H. K. Bowen, and D. R. Uhlmann, in *Introduction to Ceramics*, Vol. 4, Wiley-Interscience, New York 1976, 99.

[52] S. Fan, G. Wu, Y. Zhang, G. Chai, Z. Ma, J. Qiu, G. Dong, and J. Heo, J. Am. Ceram. Soc. **97**, 173-178 (2014).

[53] T. Hayes, L. Lurio, J. Pant, and P. Persans, Phys. Rev. B **63**, 155417 (2001).

Figures and Captions

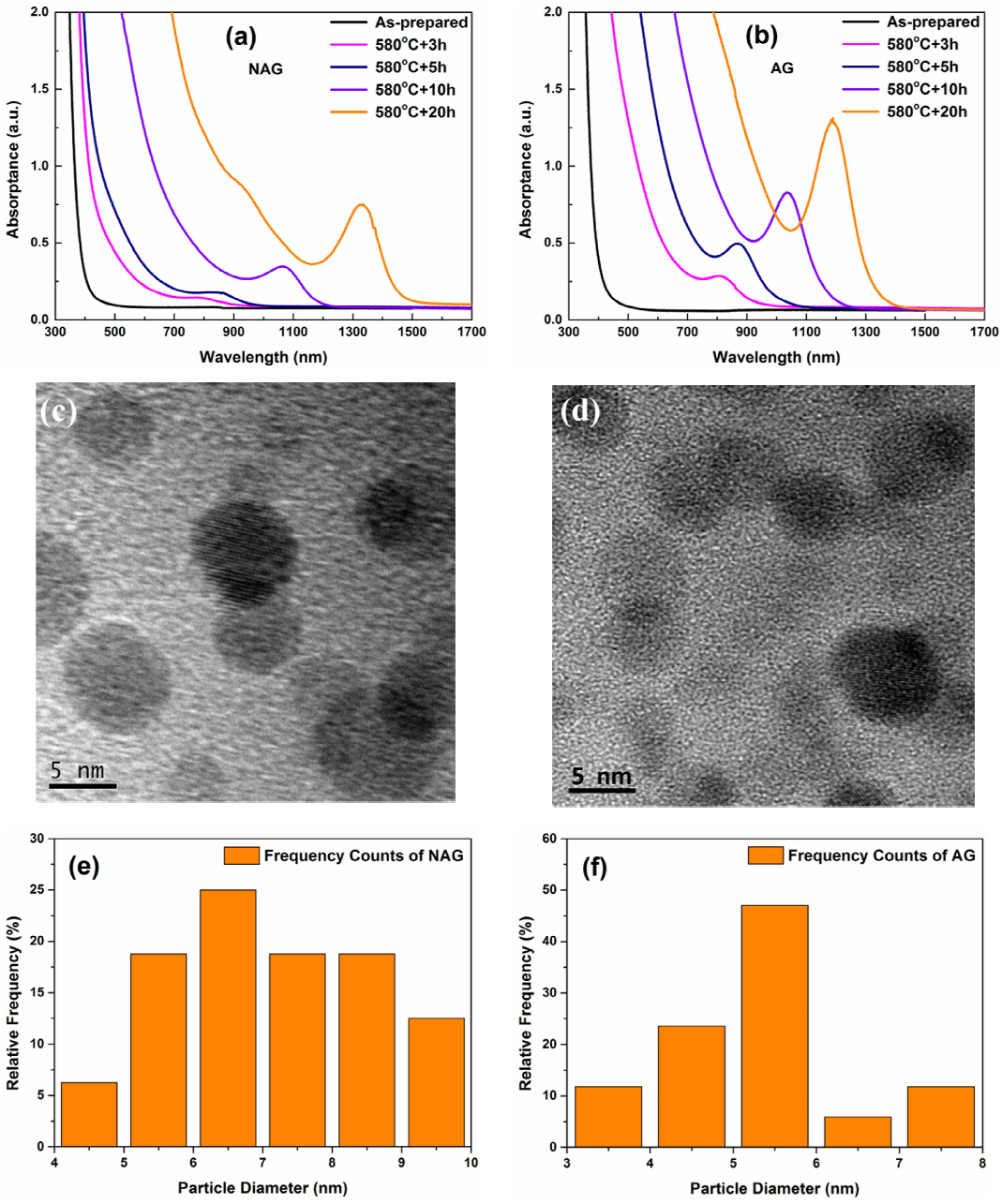

Figure 1 Absorption spectra of PbS QDs in NAG (a) and AG (b) heat treated at 580 °C for different durations. TEM images of the PbS QDs in NAG (c) and AG (d) both heat treated at 580 °C for 20 hours. (e) and (f) are the histograms of the size distribution of the QDs in (c) and (d), respectively.

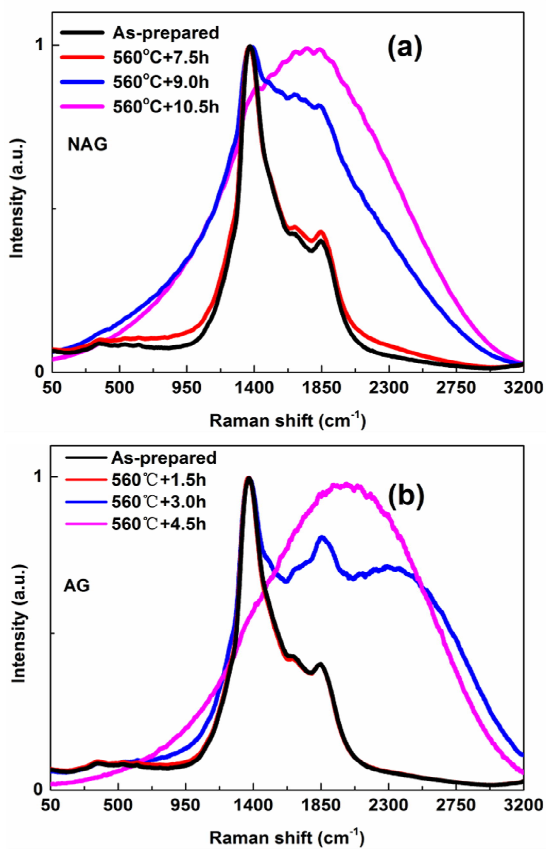

Figure 2 Normalized confocal Raman spectra of NAG (a) and AG (b) both heat treated at 560 °C for different durations.

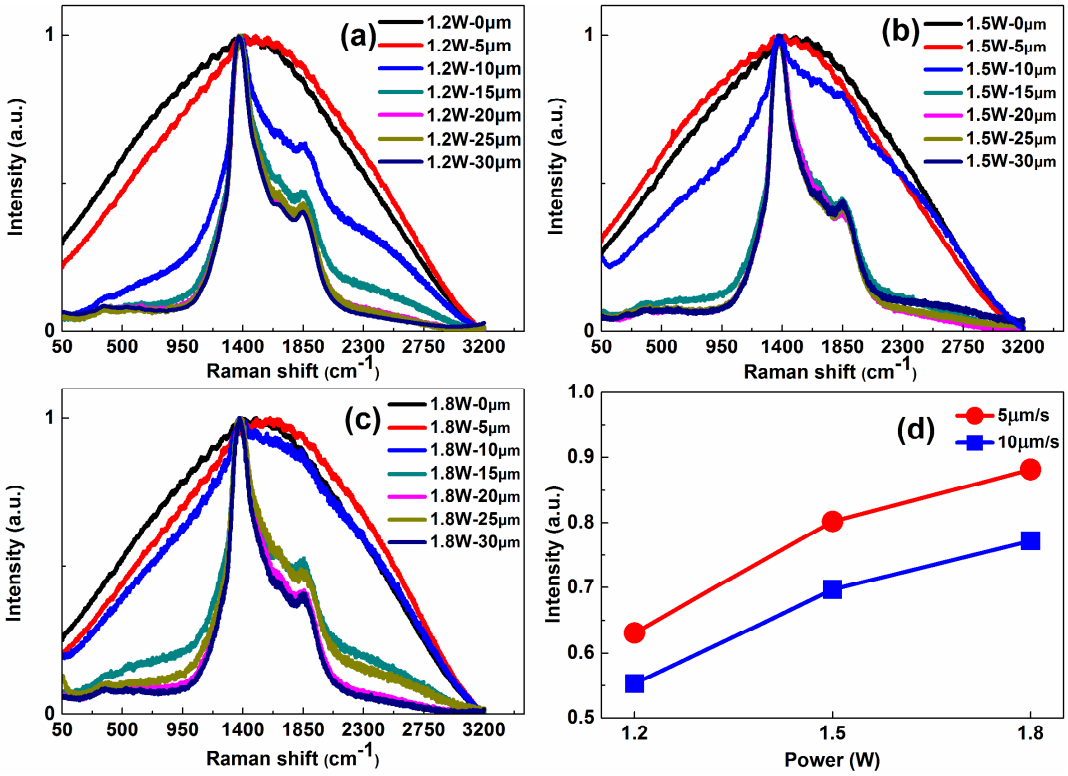

Figure 3 Normalized confocal Raman spectra for NAG irradiated with laser power 1.2 W at speed of 5 μm/s (a), 1.5 W at speed of 5 μm/s (b) and 1.8 W at speed of 5 μm/s (c). (d) The intensity of 1840 cm^{-1} to 1375 cm^{-1} for the point 10 μm to the focal center at scanning speed of 5 μm/s and 10 μm/s both as a function of laser power.

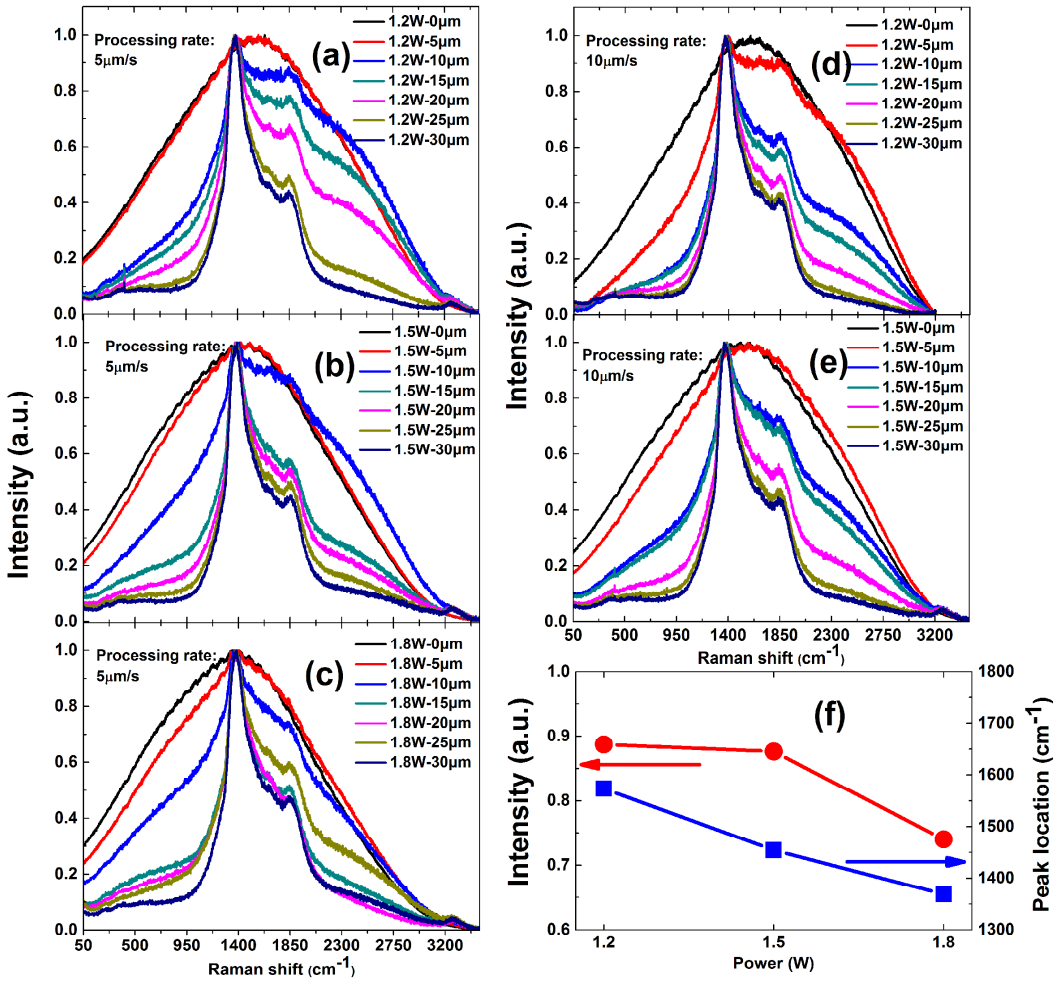

Figure 4 Normalized confocal Raman spectra for AG irradiated with laser power 1.2 W at speed of 5 μm/s (a), 1.5 W at speed of 5 μm/s (b), 1.8 W at speed of 5 μm/s (c), 1.2 W at speed of 10 μm/s (d), and 1.5 W at speed of 10 μm/s (e). (f) The Raman peak location and the intensity of 1840 cm^{-1} to 1375 cm^{-1} for the point 10 μm to the focal center at scanning speed 5μm/s both as a function of laser power.

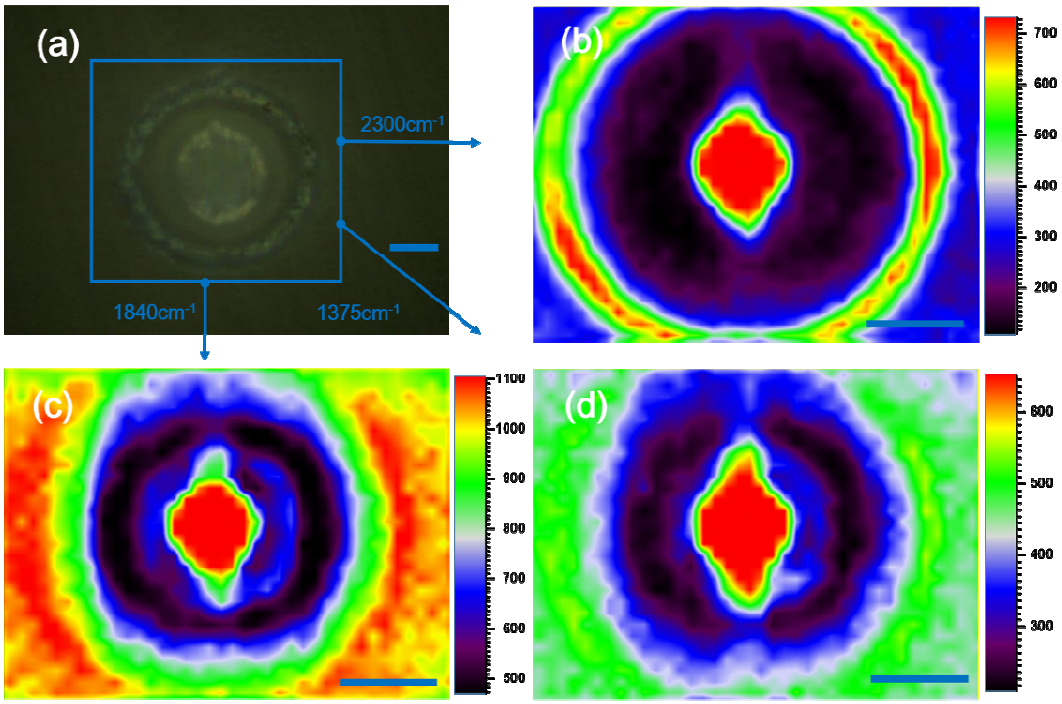

Figure 5 Optical microscope image (a) and Raman mapping for Raman peak 2300 cm^{-1} (b), 1840 cm^{-1} (c), 1375 cm^{-1} (d) of $AgNO_3$ doped glasses irradiated with laser power 1.8 W at speed of 5 μm/s. The box and the arrows in (a) are guide marks for Raman mapping zone. The blue scale bars in (a), (b), (c) and (d) all represent 20 μm.

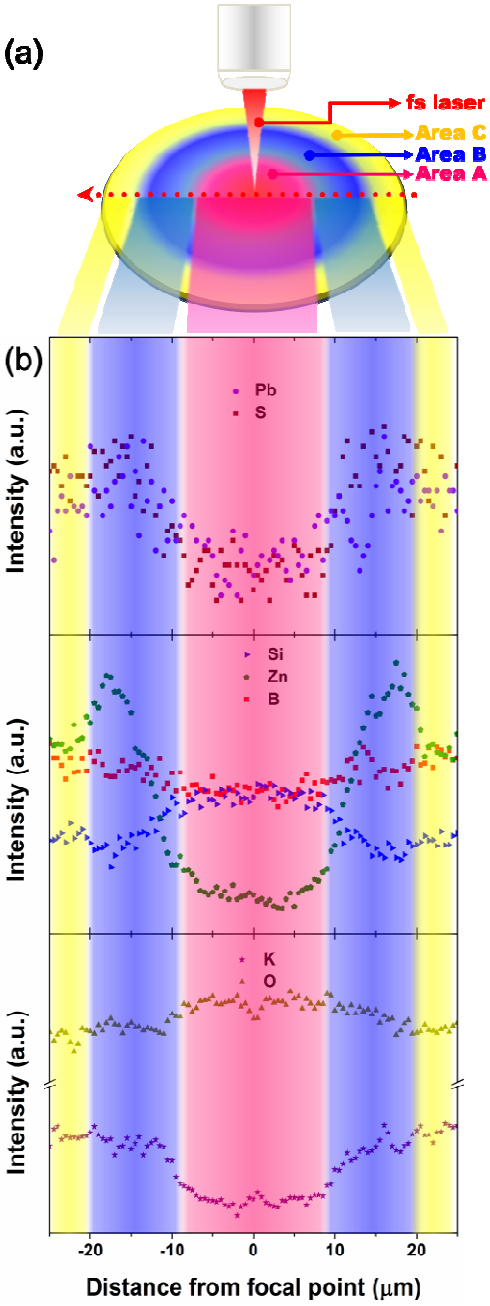

Figure 6 (a) Schematic illustration for the formation of three characteristic zones in the irradiated area. (b) Ion distribution around the focal center in AG after irradiated with laser power 1.8 W at scanning speed of 5 μm/s, as measured by EPMA. The horizontal dotted arrow in (a) is guide mark for eyes and it shows the detecting direction of EPMA.

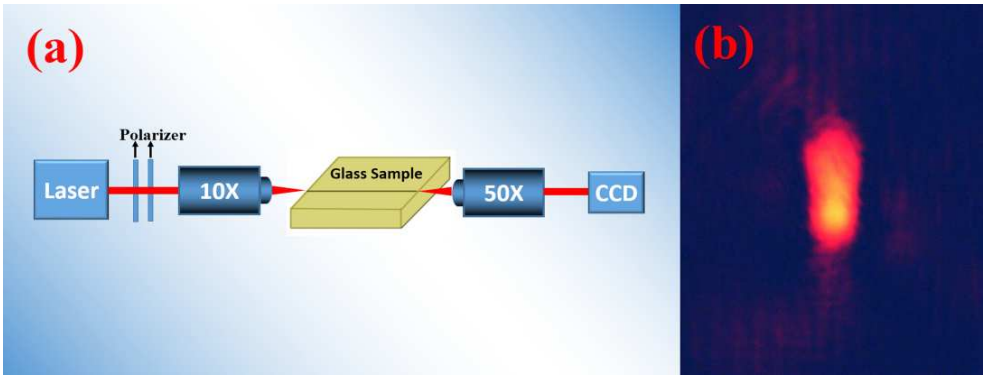

Figure 7 (a) A sketch of the end-face coupling experiment setup. (b) Beam cross section of the output 632 nm signals from a 10 mm long waveguide.

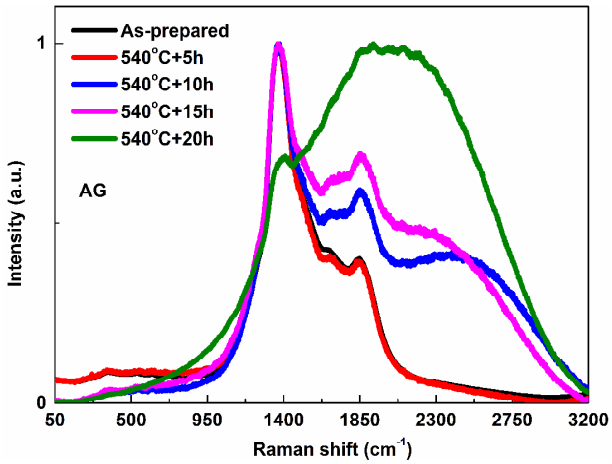

Figure 8 Confocal Raman spectra of the as-prepared AG heat treated at 540 °C for different durations.

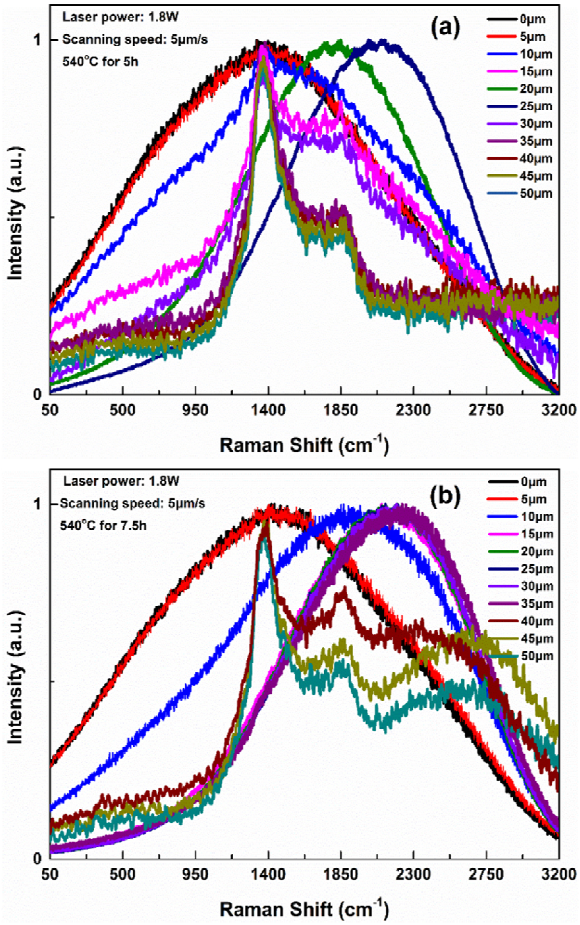

Figure 9 Confocal Raman spectra of the irradiated area (irradiating laser power is 1.8 W, scanning speed is 5 μm/s) of AG heat-treated at 540 ^{o}C for 5 hours (a) and 7.5 hours (b).

Graphical Abstract

Selective micron-region (diameter: ~30 μm) control of PbS QDs in a waveguide directly written with femtosecond laser in the glass matrix is confirmed with confocal Raman spectra. Adjustable photoluminescence band (from ~800 nm up to ~1100 nm) of the QDs in the waveguide can be precisely controlled in the irradiated zone.